SUSY TRANSITIONS IN COMPACT OBJECTS

by

IRINA ANATOLIEVNA PEREVALOVA

A DISSERTATION

Submitted in partial fulfillment of the requirements
for the degree of Doctor of Philosophy
in the Department of Physics and Astronomy
in the Graduate School of
The University of Alabama

TUSCALOOSA, ALABAMA

2010

ABSTRACT

In the standard model, energy release in dense stars is severely restricted by the Pauli exclusion principle. However, if, in regions of space of high fermion degeneracy, there is a phase transition to a state of exact supersymmetry(SUSY), fermion to sfermion pair conversion followed by radiative transitions to the Bose ground state could lead to a highly collimated gamma-ray burst.

We calculate the cross section for $ee \rightarrow \tilde{e}\tilde{e}$ in a SUSY bubble and construct a monte carlo for the resulting sfermion amplification by stimulated emission.

We construct a collective models for the nuclei and calculate the energy output for the reactions on nuclear synthesis in the region of supersymmetric matter.

To my daughter

ACKNOWLEDGMENTS

I am pleased to have this opportunity to thank many people who have helped me with this dissertation. There are no words to express my gratitude to all of them as much as they deserve.

First of all, I am most indebted to Dr. Clavelli, my scientific supervisor and the chair of the dissertation committee, for his guidance, help, kindness and eternal patience. It was my privilege to work with him. I hope that we will continue to collaborate in future.

I would also like to thank all of my committee members, Dr. Stanley Jones, Dr. Philip Hardee, Dr. Allen Stern, Dr. Benjamin Harms, Dr. Ion Stancu, Dr. Alexander Frenkel for finding the time in their busy lives to be in this committee, for their invaluable input, questions and corrections.

I would like to thank all the faculty members of Physics and Astronomy Department of the University of Alabama whose work and dedication to science and teaching are the best examples to follow. I cannot express how much I learned from them.

My work would never be completed if I would not have support of my friends: Julia Shamshina, Joshua Davidson, Sarah Higdon, and the one who wished to remain unnamed. Without them my way to finish line will be so much harder. They offered me their friendship, their hands, their hearts. They gave me comfort and shelter, and ground to start over in my life. I also want to thank my far away friends Anna

Pavlova and Alexander Balyan, whose support allowed me to come back to America to finish my dissertation.

I will be always thankful to my family, who was always there for me, my mom, my dad, my little brothers. One of them, Denis Perevalov, finished his dissertation before me but I still love him the same. And last but not least, I want to thank my daughter, Elena Perevalova, who is my inspiration in life, and without whom I will not be here. .

CONTENTS

ABSTRACT ii

DEDICATION iii

ACKNOWLEDGMENTS iv

LIST OF TABLES. viii

LIST OF FIGURES ix

INTRODUCTION 1

1 Introduction and Motivations 3

1.1 GRB: history of observations 3

1.2 GRB origin models 11

1.3 Proposed Model 15

1.4 Astronomical objects 16

2 Supersymmetry 18

2.1 Interlude 18

2.2 Constructing the Supersymmetric Lagrangian 19

2.3 Feynman Rules 22

3 Calculations of $ee \to \tilde{e}\tilde{e}$ processes 25

3.1 Electron-*s*electron scattering 25

3.2 Event generation 30

4 Nuclear Calculations 39

4.1 Nuclear models 39

4.1.1 Liquid Drop model 39

4.1.2 Shell model 44

4.1.3 Fermi gas model 46

4.2 Calculations 49

5 Discussion and Conclusions 56

REFERENCES 59

List of Tables

3.1 *S*electron momentum and angular distributions showing the effect of boson enhancement. In this run the occupation numbers are incremented by two at each throw of the dice 36

4.1 Parameter sets for liquid drop model of nuclei 41
4.2 Total nuclear energies (in MeV) for different sets of parameters . . . 43
4.3 Total nuclear energy releases (in MeV) for different models and sets of parameters 51
4.4 Nuclear fusion reactions and their energy outputs in SUSY state for different sets of parameters of liquid drop, shell and Fermi gas models (MeV) 52
4.5 Stability of different isotopes of iron nucleus. Parameters' sets are the same in the chapter. Positive number for energy release (in MeV) implies decay, whereas negative number corresponds to stability against the decay mode. F=fermionic state of nucleons, ordinary matter; B=bosonic state of nucleons, supersymmetric matter 55

List of Figures

1.1 Vela satellite signal. The first detection of GRB. 4
1.2 BATSE 2704 GRBs 7

2.1 Feynman rules for electron-selectron-photino interaction and photino propagators. 24

3.1 Feynman graphs for the conversion of an electron pair to *s*electrons via photino exchange 26
3.2 Angular distribution after $6 \cdot 10^5$ throws, showing effect of Bose enhancement. In this run the bins are incremented twice at each throw. 37
3.3 Polar angle distribution for conversion of those electron pairs whose center of momentum is that of the star. One quadrant of the angular space is shown with a balancing *s*electron jet in the opposite direction. 38

Introduction

From the very moment of discovery, γ-ray bursts (GRB) became a very fascinating subject for study. Although this phenomena has been observed for four decades, the origin of such extraordinary events is yet to be discovered.

In our research, we propose one possible explanation of the phenomena. We support our proposal with detailed theoretical calculations and computer simulations which give us confidence to consider the proposed model as consistent.

The structure of the dissertation is the following: in the first chapter, after a brief introduction to the history of the GRB, we give a description of existing models of GRB origin, pointing out, however, the reasons why we cannot accept the models entirely. Then we give a review of the astronomical objects that will be important for our model. Finally in the end of the chapter we introduce our model.

Chapter two is entirely theoretical. After a brief introduction of supersymmetry (SUSY) we provide the apparatus we used in later calculations.

In chapter three we present the calculations for the fermion $\rightarrow$ s-fermion transition cross-sections for the Dirac sea and results of Monte Carlo simulations for these transitions.

In chapter four we present different collective nuclear models and the results of numerical evaluations of the energy release during the SUSY transition. Energy balance for possible nuclear reactions is also provided in this chapter.

Finally, we present our conclusions in chapter five.

Chapter 1

Introduction and Motivations

1.1 GRB: history of observations

The discovery of gamma-ray bursts (GRBs) is an excellent example of serendipity, or a fortunate accident, in science. If it had not been for the Cold War that began in the 1950's between the two super powers of the Soviet Union and the United States, these cosmic events may not have been detected until many decades later.

The history of the exploration of GRBs began in October 1963 with the launch of the first pair of U.S. Air Force "Vela" satellites (part of the Vela-Hotel project) for monitoring nuclear testing by the Soviet Union and any other countries with nuclear capabilities. These satellites were equipped with X-ray, gamma-ray, and neutron detectors. During a nuclear explosion, most of the energy released is in the form of X-rays that are detected as an X-ray flash. The typical flash curve has distinctive two-maximum shape. The first, short and intense flash lasting around 1 millisecond, is followed by a second much more prolonged and less intense emission of light taking a fraction of a second to several seconds to build up. Simultaneous detection of γ-rays and, following that, a neutron burst, provides the corroborative evidence that a

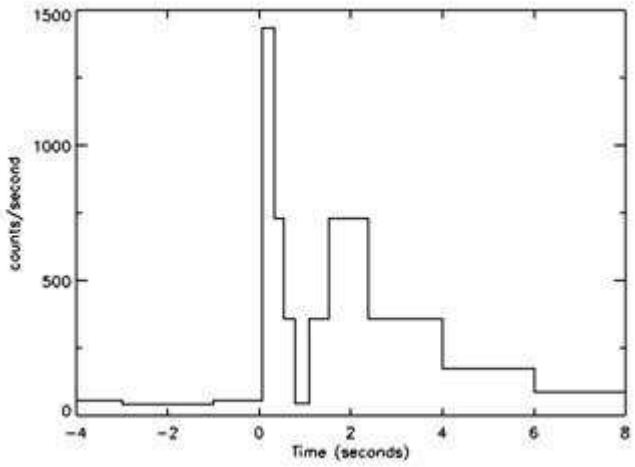

Figure 1.1: Vela satellite signal. The first detection of GRB.

nuclear event has been authentically observed.

In 1965, two years after the launch of the first pair of "Vela" satellites, five more pairs of satellites in this series were placed into orbit. These satellites were engineered as pairs to collect complementary data from both of the Earth's hemispheres (with one of the pair satellites collecting data from an "a" portion of one hemisphere and its pair collecting data from a "b" portion of the other hemisphere). When a nuclear explosion occurred, a signal from one of the satellite pairs was used to determine where the explosion occurred. The exact location of the nuclear explosion was ascertained by triangulation of data added from another of the "Vela" satellites.

On July 2, 1967 the Vela 4a and the Vela 4b satellites registered a puzzling event that was initially thought to be a mistake, which proved to be the first evidence verifying the existence of gamma-ray bursts. On this seminal date - which marks the beginning of the scientific study of gamma rays - instruments on both of these

satellites registered simultaneous highly energetic gamma flashes (see Figure 1.1). The energies and durations of the events were unusual and were not accompanied by any other types of radiation typical for a nuclear explosion (like high energetic neutron flash). At first scientists suspected an instrument error. After repeated detection of similar events, they concurred that the signals were valid. Since the flashes registered simultaneously on a pair of instruments over different hemispheres, the only feasible explanation was (and still is) that the flashes originated from an extra-terrestrial source. The detection of gamma-ray bursts from the "Vela" satellites remained classified by the U.S. government until 1973 when the information was published [1].

On March 14, 1971 NASA launched the IMP6 (Interplanetary Moving Platform) satellite with a gamma-ray detector aboard. Although the main purpose of the instruments was not to detect GRBs, the instruments observed and collected data about them while monitoring solar flares. (Unfortunately, the γ-instrument failed on September 26, 1972.) In September 1971 the Seventh Orbiting Solar Observatory (OSO-7) was launched. It carried an X-ray telescope designed to accurately measure the highly energetic part of the X-ray spectrum from sources across the sky and monitor gamma rays.

Only after the declassification of the Vela data in 1973 did it become possible to publish findings concerning the 16 bursts that were observed by Vela 5a,Vela 5b, Vela 6a, and Vela 6b between July 1969 and July 1972. In the following year, data from the Soviet Konus satellite were published, confirming the detection of the same bursts of gamma rays. With the publication of both the U.S. and Soviet data that had been

independently collected and confirmed, the era of active GRB research began.

In 1976 a set of gamma-ray detectors were placed on a spacecraft named the Interplanetay Network (IPN), which was designed to study the Solar system. These detectors worked in unison to locate gamma-ray bursts through a process of triangulation. By localizing the sources of GRBs to a few arc minutes, the IPN showed that these sources were not from a previously known source, such as an X-ray emitter. (The IPN continues today as a part of a larger project).

Even though the GRB events were observed on a regular basis (on average once a day) their origin remained unknown. No obvious sources of gamma-ray emission were observed near the areas where GRBs were detected.

On March 5, 1979 an unusual gamma-ray transient was found, later localized to the N49 supernova remnant in the Large Magellanic Cloud [2]. This caused a controversy that lasted for over a decade; one side of the astrophysical community believed it to be an accidental coincidence. They believed that GRBs could not come from a source as distant as the LMC galaxy since the energies of the event creating the GRBs would be too large. The opposing side maintained the opinion that two classes of gamma radiation sources exist, and that this is a separate occurrence from GRBs. Later study of Soft Gamma Repeaters by ASCA (Advanced Satellite for Cosmology and Astrophysics) proved the latter to be correct [3].

April 5th, 1991 became an important day in the study of GRBs. NASA put into orbit the Compton Gamma Ray Observatory. For a long time this mission was the major supplier of experimental data for the GRB research community. Included in its payload was the Burst And Transient Source Experiment (BATSE) instrument,

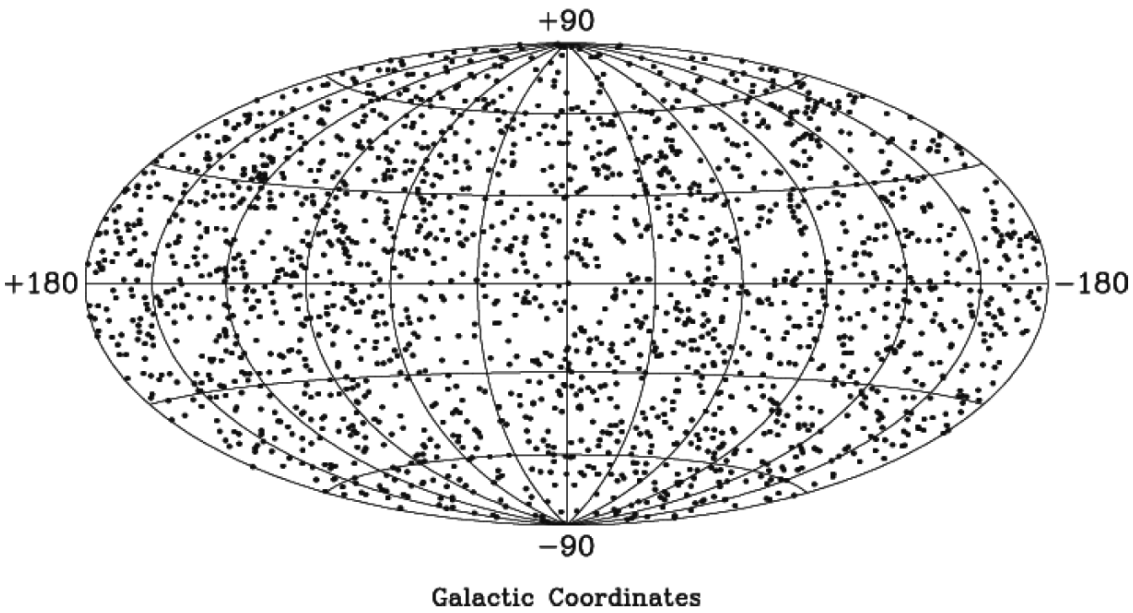

Figure 1.2: BATSE 2704 GRBs

which was dedicated solely to GRB studies and detected over 2,700 gamma-ray bursts in nine years.

BATSE data showed that GRBs are uniformly distributed across the sky (see Figure 1.2), and not concentrated along the plane of the Milky Way, thus proving that the GRBs originate far outside the Milky Way galaxy. As a result, this suggests that GRBs should have enormous energies associated with them in order to be detectable across the entire observable universe [4].

This knowledge sparked a paradigm shift. Gamma-ray bursts were now viewed as cosmological in origin. With no commonly accepted theoretical explanation of the phenomena, GRB research became one of the frontiers of astrophysics.

With several instruments in orbit, it became important to have a uniform way of referring to the events. So the standard naming for a GRB became the following:

GRB + the last two digits of the year + two digits signifying the month + 2 digits signifying the day of the month + an alphabetic letter designating the numerical order of an observed event for that month. So, for example, the third GRB on January 16, 2012 will be GRB0120116C.

Once put in orbit, more elaborate instruments allowed not only the detection of GRBs, but also provided possibilities for the study of the structure of the spectrum of these events. More focused studies discovered another special feature of the bursts. Most of the bursts have a trail of lower energy radiation originating from the same region of space where the GRB was detected and, thus, is a characteristic associated with these bursts, called the afterglow [5].

The launch of the BeppoSAX satellite on April 30, 1996 commenced the era of studying GRB afterglows. Looking at GRB997228 (this is from outmoded notation where the second "9" meant that the data was taken by BeppoSAX and 228 is the order number) astronomers detected an X-ray afterglow associated with a gamma-ray burst for the first time [6].

In 1999 the afterglow of GRB990123 was detected within seconds of the initial burst [7]. Based on detailed analysis, astronomers determined that the energy was channeled in narrow jets. As a result, the detection of a GRB is possible only if the jet is aimed along the observer's line of sight. The energy output of this event was estimated at 10^{50} erg, which is 1,000 times more luminous than quasars and 10^{17} times more luminous than the Sun. Hence, finding the source of such an enormous amount of energy became an important issue.

Analysis of the emission lines from the afterglow of GRB990705 showed an iron-

absorption feature that is characteristic of a supernova[1] [8]. This direction of the GRB origin explanation remained dominate, especially after observation of iron lines from the GRB991216 afterglow made by the Japanese X-ray satellite ASCA and by NASA's Chandra X-ray Observatory that helped pinpoint a distance to the burst[2] [9].

This discovery lead to research efforts on supernovae as a reasonable prospect for the source of GRBs. To continue research in this direction, NASA launched the High Energy Transient Explorer (HETE) on October 9, 2000. This MIT-built international project was designed to detect and rapidly pinpoint the location of gamma-ray bursts.

Detailed analysis of the GRB011211 afterglow found evidence of silicon, sulfur, argon, and other elements in the shell of gas surrounding the burst [10]. Such a spectrum is typically associated with a supernova. On October 4, 2002 HETE detected a burst and pinpointed its location. Scientists were able to communicate the coordinates of the burst quickly enough that with coincident data from other telescopes, scientists found evidence for the death of a massive star and the birth of what appears to be a black hole in its place[3] [11]. Because of such success, more instruments for detailed research were put into orbit. On October 17, 2002 the European Space Agency launched INTEGRAL (International Gamma Ray Astrophysics Laboratory), a gamma-ray observatory containing a burst detector.

On December 23, 2002 HETE detected the afterglow of a GRB that by all previous

[1]Supernova - explosion of the star during which its luminosity increases in orders of magnitude. See next section for more discussion.

[2]To determine the distance to the source one should determine the red shift of known element lines and by red shift - evaluate the distance.

[3]Leading theory of origin of long duration GRBs is collapsing massive star that that converting into a black hole.

observations was supposed to be "dark." These GRBs are short in duration as well as their afterglows. Typical short duration bust lasts less then two seconds (opposing the long duration bursts that last up to twenty seconds). Such bursts, accounting for roughly half of all GRBs, were thought to be devoid of optical afterglows [12]. Since this afterglow disappeared within 2 hours, if the afterglow had not been detected as quickly as it was, this GRB would have been labeled "dark." Perhaps no burst is truly dark if it is observed in its initial state.

On March 19, 2003 NASA announced compelling evidence that the spectrum of long-duration bursts (which is the ongoing energizing of the burst afterglow for more than half an hour after a burst) are formed from the death of massive stars and the simultaneous creation of a black hole [13]. This observation is supported by data from GRB030329, GRB050315, GRB050502B, as well as from the quite recent data from GRB080319B [14, 15, 16, 17].

On November 20, 2004 NASA launched SWIFT, the first-of-its-kind multi-wavelength observatory dedicated solely to the study of gamma-ray bursts. It has three instruments working together to observe GRBs and afterglows in the gamma-ray, X-ray, optical, and ultraviolet wavebands. Currently most of the GRBs are identified and observed first by SWIFT [17].

The most modern update of the progressive improvements in GRB instruments was launched on June 11th, 2008. The Gamma Ray Large Area Space Telescope (GLAST, now known as FERMI) carries an instrument to detect gamma-ray bursts with photons thousands of times more energetic than SWIFT is capable of detecting. FERMI has already started data collection. Currently, FERMI is working in sky

survey mode, pinpointing the sources of GRBs for detailed observation from telescopes at observatories.

1.2 GRB origin models

Although there has been intense scientific effort to understand the bursts, their origin remains elusive. There have been at least 200 distinct theories to explain the origin of the bursts [18].

The first theories started to appear even before the Vela observation disclosure in 1973. The first two decades of searching for answers concerning the GRB puzzle can be called the "golden era" for theoreticians. Except for a required description of the observed frequency of GRB events, there were no limitations imposed on the theories. A wide variety of theoretical models have been proposed, and these can logically be divided into three groups: Solar system based, Galaxy based, and those of cosmological origin. It should be noted that proposed heliocentric models were almost immediately excluded because of inconsistencies in observations and suggested mechanisms. The only source of GRBs in these models is the Sun. The modern state of Solar observations and studies does not provide any support for these models. BATSE provided the evidence to discontinue these studies entirely.

For the first few decades of GRB study, the Galactic approach was dominant, which made seemingly good sense in accounting for the huge energy output of events. Since the source of the GRB was never directly observed, early on the two main candidates for the source were neutron stars (NS) [19] or white dwarfs (WD) [20]. There were numerous theories that postulated the involvement of either a neutron star

or a white dwarf due to accretion of material from a companion (WD, NS or ordinary star), starquakes, and collision of a NS with a comet or asteroid. All of the above models imply isotropic energy distribution from objects in our Galaxy. However, as data from BATSE's more sensitive instruments made an appearance, these models started to show inconsistencies.

This apparent isotropic distribution of GRBs became a difficult observation to explain. Since the Sun is offset from the Galactic Center by some 30,000 light years, the only way out of anisotropy is through the hypothesis that neutron stars occupy a massive invisible halo around our Galaxy that is more than half a million light years in radius [21]. But even in this scenario, a small deviation from isotropy is to be expected because of Solar system Galactic offset. To take this expected deviation into account and to fit with data from more recent observations, the Galactic model needed a major revision at the very least. The question of whether the Galactic approach should be altogether abandoned in favor of a theory that postulated GRBs as cosmological events became timely because the Galactic Model did not contain the necessary parameters to explain the observed isotropy.

When the bursts' sources were taken outside the Galaxy, the question of the energy source of GRBs looms large. In order for current instruments to be able to observe the experimental flux of a GRB , the energy output at a source needs to be many orders of magnitude larger than any known source. To be consistent with current observations, the following explanation was suggested: GRB emission is highly collimated, and only those that are pointed toward the Earth can be observed. This approach supports the hypothesis that GRBs are a very common event, since we observe up to several

GRBs a day.

Most models of GRB origin link supernovae and GRBs together. GRBs are believed to occur when a blast wave of material is produced inside a collapsing star about to undergo a supernova explosion. Both the gamma rays and the blast wave of stellar material erupt from the star - the gamma rays necessarily travel at the speed of light while the stellar material travels just a little slower - jetted along an axis. From these observations, a question fundamental to our new theory materializes: how frequently do GRBs occur? Or how common are these events?

While there is, on average, only one supernova per galaxy per century, there are something on the order of 100 billion galaxies in the observable Universe (which refers to the part of the Universe from which light has had time to reach us). Taking a very conservative estimation for the age of the Universe as 10 billion years[4], one could derive a figure of 1 billion supernovae per year. That comes to about 30 supernovae per second in the observable Universe!

For the supporters of the supernova model, the GRB030329 event was perfect example [14]. The optical spectrum of the afterglow was nearly identical to that of supernova SN1998bw. In addition, observations from X-ray satellites showed the same characteristic signatures of "shocked" and "heated" oxygen which are also present in supernovae. Thus, astronomers were able to determine that the "afterglow" light of a relatively close gamma-ray burst (located only 2 billion light years away) resembled a supernova.

What is almost certain is that the core of the star involved in a given supernova

[4]Modern data predicts age of the Universe is 13.7 billion years

is massive enough to collapse into a black hole (rather than a neutron star) and data from GRB021004 supports this tenet of the model of the supernova origin of GRBs [13].

However, the remaining problem for this model is jet formation. Supernova collapse leads to isotropic energy release. To accommodate jet formation this model needed to be altered. In order to create a jetted structure an internal engine was proposed. The engine creates initial jetted bursts in opposite directions. These primordial jets pass through the stellar material creating the collimated jets with a train of the particles native to the stellar environment. As a result, the afterglow will match the spectrum of a supernova.

The most important assumption in the model above is the existence of a mysterious internal engine that ignites the stellar material. The nature and existence of this initiating force is still unknown.

Among the astronomical models for GRB formation, the most popular are collapsar and merging binary system scenarios [22, 23]. A collapsar is a massive rotating star ($M_{ms} > 25M_{sun}$) the core of which collapses to form a black hole. In a rapidly rotating star, the accretion of the rest of the star into the newly-formed black hole may produce a long-duration gamma-ray burst accompanied by a Type Ib/c supernova. Since collapsars naturally form jetted explosions beamed to a small fraction of the sky, the energetic requirement is typically hundreds of times less than the observed "isotropic equivalent energy." Recent observational evidence of both the close association of well-localized GRBs with star-forming regions, and possible direct links between GRBs and supernovas, supports the collapsar model.

Another possible, but more exotic, astronomical model of GRB formation is the merger of a binary system [23]. Most models consider the merger of black holes, neutron stars and white dwarfs in any combination of two. Even though the energy output for such systems approaches the observable GRB limit, the population of such systems in the observable Universe is believed to be too small to explain the majority of GRB events.

1.3 Proposed Model

The proposed model is based on the yet to be observed supersymmetry (SUSY).

It has been shown [25] that in the presence of matter with high densities it may become possible to have a transition from the vacuum of broken supersymmetry (our Universe) to the vacuum with restored supersymmetry. This transition creates a bubble of the new state inside the super dense matter which immediately starts to expand, since the minimal energy principle favors the supersymmetric state. The growth of the bubble stops as its boundary hits the surface of the object. Subsequently, a supersymmetric object continues to exist in the bounded state forever, or it collapses because it lacks the fermionic pressure that was opposing the gravitational pressure in regular matter.

In this work, it is shown that during the process described above, a gamma ray burst naturally appears during the phase transition inside compact astronomical objects such as white dwarfs and neutron stars which possess the densities required for SUSY transition. Since the new state is bosonic, jet formation happens naturally in processes similar to the Bose enhancement in lasers. It is also shown that

1. The energy output for the GRBs in our model is comparable to GRBs that have been observed.

2. The duration of the GRB bursts in our model is within the parameters of observed GRBs.

1.4 Astronomical objects

Neutron stars and white dwarfs are two possible outcomes for the last stage of a star's evolution, but they are not the only possible outcomes. Starting from the hydrogen-rich young stage, every star undergoing the chain of nuclear reactions that starts from the H-He cycle[5] ends with a carbon creating state. Following that, depending on the mass of the star, it could end up in the equilibrium state of a white dwarf, or pass through the CNO cycle [26] and end up in the neutron star stage.[6]

White dwarf stars are the final stage of evolution of stars with final mass up to 1.4 $M_{\odot}$. Observations have shown that most stars end up as white dwarfs. The total mass and pressure inside them is not enough to trigger the CNO cycle. After exhausting all of the hydrogen-helium energy resources, such stars fall into darkness radiating all the remaining energy through cooling. As a result, they end up as carbon rich stellar

[5]Standard H-He cycle, also known as PP I , II, III chains, converts hydrogen into helium. It is the first major player in a stars' nucleosynthesis.

[6]Standard CNO cycle runs in heavier stars and produces helium-4 from hydrogen. Most active branch of the reaction is

$$\begin{aligned}
{}^{12}\mathrm{C} + {}^{1}\mathrm{H} &\rightarrow {}^{13}\mathrm{N} + \gamma \\
{}^{13}\mathrm{N} &\rightarrow {}^{13}\mathrm{C} + e^{+} + \nu_e \\
{}^{13}\mathrm{C} + {}^{1}\mathrm{H} &\rightarrow {}^{14}\mathrm{N} + \gamma \\
{}^{14}\mathrm{N} + {}^{1}\mathrm{H} &\rightarrow {}^{15}\mathrm{O} + \gamma \\
{}^{15}\mathrm{O} &\rightarrow {}^{15}\mathrm{N} + e^{+} + \nu_e \\
{}^{15}\mathrm{N} + {}^{1}\mathrm{H} &\rightarrow {}^{12}\mathrm{C} + {}^{4}\mathrm{He}
\end{aligned}$$

objects with traces of oxygen inside the interior.

In the case of a more massive star (less then $25M_{\odot}$), stages similar to the white dwarf ancestor will be passed through, but it will continue to generate energy in carbon, oxygen and silicon nuclear burning cycles. Ultimately the star will undergo a gravitational collapse and will become a neutron star with an average mass of 1.35-2.1 $M_{\odot}$.

These two final stages of stellar evolution are not the only possible, but are the important stages that our model is concerned with. Both white dwarf and neutron stars lose thermal energy through radiative cooling. This leads to a maximal possible contraction of the stellar material, especially for neutron stars, and as a result these stars become the densest objects in the Universe (apart from black holes). This extreme density results in enormous pressure in the interior of the star and increases the possibilities for SUSY transition.

Chapter 2

Supersymmetry

2.1 Interlude

Modern particle physics accepts the standard model (SM) as a launch pad for the search of the ultimate theory of matter just as Newtonian Gravity is the starting point for modern gravitational theory. Although the SM (which combines the theory of electroweak interactions and quantum chromodynamics), agrees with experimental results and has rather remarkable predictability, it lacks the beauty of the expected theory. The model has twenty-nine free parameters (ten of which were introduced to accommodate the neutrino oscillations), does not include gravity, and poses several fine-tuning problems, most famous of which is the Higgs/hierarchy problem [27]. No wonder that physics beyond the SM became one of the most popular branches of modern particle physics. In our opinion, the most natural extension of the SM could be found in theory of Supersymmetry.

Supersymmetry (SUSY) pairs bosons with fermions, making them superpartners. In ideal, non-broken SUSY, one would observe particles with the same mass, electric charge and every quantum number except spin, hence different statistics. However,

we have, so far, not observe such pairs. The only logical outcome of such phenomena is that our world exists in broken SUSY. That means that all superpartners for the SM particles belong to the heavy mass part of the spectrum. Searches for these particles are in the plans for the Large Hadron Collider (LHC).

In this chapter we review ideas of Supersymmetry and derive the main equations that will be used for calculations in the later chapters of the work.

2.2 Constructing the Supersymmetric Lagrangian

One starts construction of the Lagrangian density for field theory from the free field (non-interacting, containing only kinetic terms) equations. The minimal supersymmetric (MSSM) content of field theory in four dimensions is a single left-handed two-component fermion ψ and its superpartner, a complex scalar field ϕ. Since the complex scalar field associated with bosons, has 2 real degrees of freedom and the fermion field has 4 degrees of freedom, one has to modify the Lagrangian by adding the additional 2-dimensional (hence, scalar) field F. Such an addition, will insure that supersymmetry transformations of a scalar field into a fermion field, and vice versa, will close. But the addition of the auxiliary field should not affect the dynamics. One can define noninteracting action according to

$$S = \int d^4x \, (\mathcal{L}_{scalar} + \mathcal{L}_{fermion})$$

An infinitesimal SUSY transformation should satisfy $\delta\mathcal{L}_{scalar} + \delta\mathcal{L}_{fermion} = 0$.

The free Lagrangian density will have the simple form

$$\mathcal{L} = -\partial^{\mu}\phi^{*i}\partial_{\mu}\phi_i - \mathrm{i}\psi^{\dagger i}\overline{\sigma}^{\mu}\partial_{\mu}\psi_i + F^{*i}F_i \tag{2.1}$$

$i = 1, 2$ - are spinor indexes and $\mu = 1, 2, 3, 4$ - space-time indexes; $\sigma^{\mu} = (\mathbf{1}, \vec{\sigma})$, where $\vec{\sigma}$ are traditional Pauli matrices. Here the first term corresponds to the scalar part of the kinetic term, the second term is the fermion part and the last term is a term for the auxiliary field.

We will now need to include the interaction into this Lagrangian. Naturally one should start from the chiral interactions leaving the gauge ones for later. In the MSSM this part of the particle spectrum is populated by quarks, *s*quarks, leptons, *s*leptons, Higgs bosons and higgsino fermions.

The most general form of the renormalizable interactions that respect supersymmetry transformations and are no greater than a power of three in the field count can be written in the form

$$\mathcal{L}_{\mathrm{int}} = \left(-\frac{1}{2}W^{ij}\psi_i\psi_j + W^i F_i\right) + \mathrm{c.c.}. \tag{2.2}$$

here we introduced the analytical function of the complex scalar fields:

$$W = \frac{1}{2}M^{ij}\phi_i\phi_j + \frac{1}{6}y^{ijk}\phi_i\phi_j\phi_k, \;\; W^i = \frac{\partial W}{\partial \phi_i} \;\; W^{ij} = \frac{\partial^2 W}{\partial\phi_i\partial\phi_j}$$

The auxiliary part of the full Lagrangian (similarly to the one in (2.1)) will have the following form: $F_i F^{*i} + W^i F_i + W_i^* F^{*i}$. All these terms together can be absorbed

into $W^i W_i^*$ so the total Lagrangian (including chiral superfield interactions) could be written as:

$$\mathcal{L}_{\text{chiral}} = -\partial^\mu \varphi^{*i} \partial_\mu \varphi_i - \mathrm{i}\psi^{\dagger i} \overline{\sigma}^\mu \partial_\mu \psi_i - \frac{1}{2}\left(W^{ij}\psi_i\psi_j + W^*_{ij}\psi^{\dagger i}\psi^{\dagger j}\right) - W^i W_i^* \qquad (2.3)$$

In the next step one should include the gauge interactions into the Lagrangian. The content of this part of the particle population is the massless gauge boson field A^a_μ and a two-component Weyl fermion gaugino λ^a. Similar to the chiral supermultiplet, matching the on- and off-shell degrees of freedom, one should introduce an auxiliary real bosonic field B^a to compensate the one degree of freedom mismatch.

That means that the Lagrangian density for the gauge supermultiplet has to have the following form:

$$\mathcal{L}_{\text{gauge}} = -\frac{1}{4}F^a_{\mu\nu}F^{\mu\nu a} - \mathrm{i}\lambda^{\dagger a}\overline{\sigma}^\mu D_\mu \lambda^a + \frac{1}{2}B^a B^a, \qquad (2.4)$$

where

$$F^a_{\mu\nu} = \partial_\mu A^a_\nu - \partial_\nu A^a_\mu + g f^{abc} A^b_\mu A^c_\nu$$

and

$$D_\mu \lambda^a = \partial_\mu \lambda^a + g f^{abc} A^b_\mu \lambda^c$$

where f^{abc} are the structure constants of the gauge group.

Now one must include cross-supermultiplet interactions into the Lagrangian. To have a gauge invariant Lagrangian one should simply replace the ordinary derivatives

in (2.3) with their covariant analog: $\partial_\mu \phi_i \rightarrow D_\mu \phi_i = \partial_\mu \phi_i - \mathrm{i} g A^a_\mu (T^a \phi)_i$. In this we used the fact that chiral supermultiplets transform under the gauge group in the ajoint representation with hermitian matrices $(T^a)^j_i$, with the rule $[T^a, T^b] = \mathrm{i} f^{abc} T^c$.

Three additional renormalizable terms that couples gauge and chiral supermultiplets that couples matter fields with gaugino and auxiliary field B need to be included in order to have all possible interactions. The full lagrangian density for the renormalizable supersymmetric theory finally will have the form:

$$\mathcal{L} = \mathcal{L}_{\text{chiral}} + \mathcal{L}_{\text{gauge}} - \sqrt{2} g (\phi^\dagger T^a \psi) \lambda^a - \sqrt{2} g \lambda^{\dagger a} (\psi^\dagger T^a \phi) + g (\phi^\dagger T^a \phi) B^a \qquad (2.5)$$

This step completes the construction of the Lagrangian.

2.3 Feynman Rules

Among all possible vertices and propagators for the MSSM we will state only those that are important for our work. In our model we will consider $ee \rightarrow \tilde{e}\tilde{e}$ transitions at tree level. The only term in (2.5) that contributes to this interaction is $\sqrt{2} g (\phi^\dagger T^a \psi) \lambda^a$.

As usual one can define a spinor as

$$\psi \equiv \begin{pmatrix} \psi_L \\ \psi_R \end{pmatrix}; \qquad \psi_{L,R} = P_{L,R} \psi; \qquad P_{L,R} = \tfrac{1}{2}(1 \mp \gamma_5); \qquad \gamma_5 = \mathrm{i} \gamma^0 \gamma^1 \gamma^2 \gamma^3$$

$$\bar{\psi} = \psi^\dagger \gamma^0; \qquad \psi^c = C \bar{\psi}^T; \qquad C = -\mathrm{i} \gamma^2 \gamma^0$$

The boson content of matter in this interaction is the *s*lepton $\tilde{e}_L$ and $\tilde{e}^+_L$; the fermion content is e and e^+; and the photino, $\tilde{\gamma}$, is the mediator of the interaction.

So the full interaction can be written as

$$\sqrt{2}\mathrm{e}\left(\bar{\tilde{\gamma}}P_L e\tilde{e}_L^* + \bar{e}P_R\tilde{\gamma}\tilde{e}_L - \tilde{\gamma}P_R e\tilde{e}_R^* - \bar{e}P_L\tilde{\gamma}\tilde{e}_R\right).$$

Corresponding to each external fermion line in the diagram, one attaches a $u(p)$ or $v(p)$ spinor. For Dirac fermions, one uses $u(p)[\bar{u}(p)]$ for an incoming[outgoing] particle state and $\bar{v}(p)[v(p)]$ for an incoming[outgoing] antiparticle state. In calculations one makes use of following summations over the spin:

$$\sum_s u(p)\bar{u}(p) = \not{p} + m\,, \qquad \sum_s v(p)\bar{v}(p) = \not{p} - m\,.$$

However, for Majorana fermions $\psi_M = \psi_M^c \equiv C\bar{\psi}_M^T$ so the combination of u and v also arise:

$$\sum_s u(p)v^T(p) = (\not{p} + m)C^T\,, \qquad \sum_s \bar{u}(p)\bar{v}(p) = C^{-1}(\not{p} - m)\,,$$

$$\sum_s \bar{v}^T(p)\bar{u}(p) = C^{-1}(\not{p} + m)C^T\,, \qquad \sum_s v(p)u^T(p) = (\not{p} - m)C^T\,.$$

Corresponding rules for the diagrams are presented in the Figure 2.1

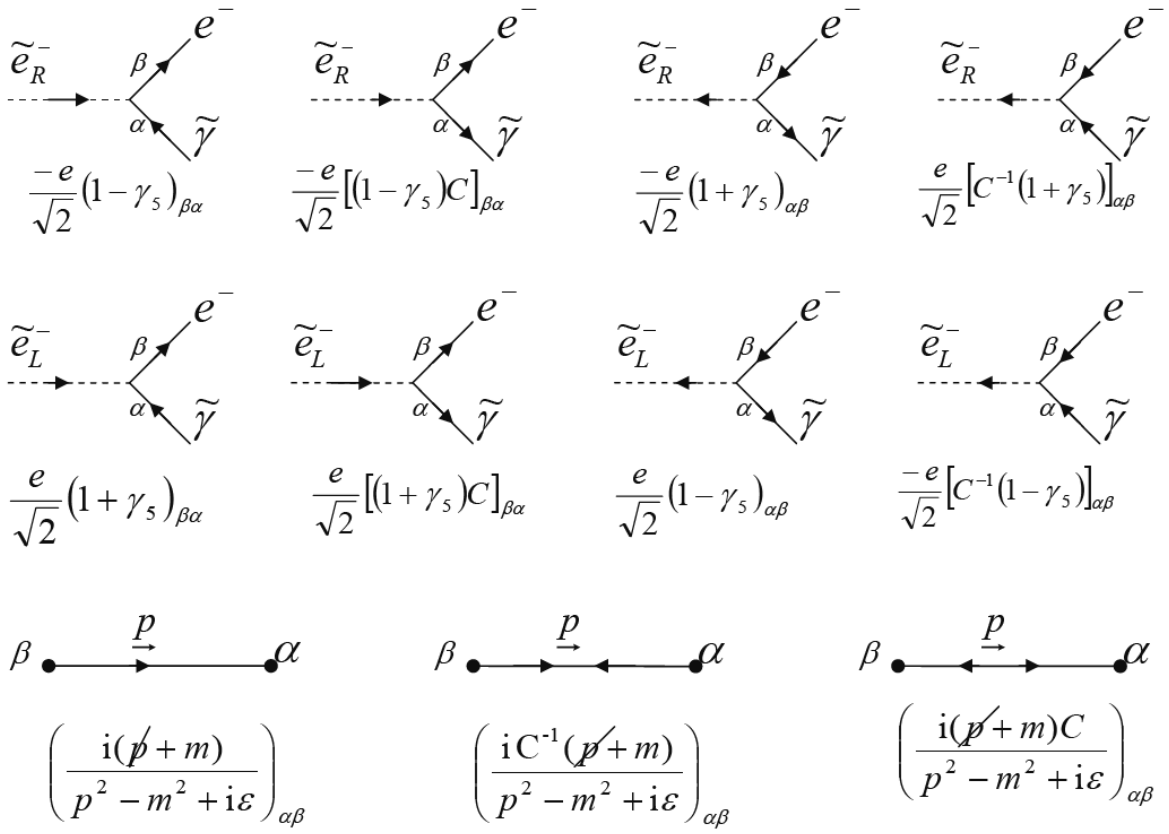

Figure 2.1: Feynman rules for electron-selectron-photino interaction and photino propagators.

Chapter 3

Calculations of $ee \to \tilde{e}\tilde{e}$ processes

The results are applicable to a possible SUSY conversion in a white dwarf which, in the broken SUSY phase, is stable against gravitational collapse due to electron degeneracy. In a neutron star, the SUSY conversion would be more complicated and the energy release would be more slow since sneutrons will not efficiently radiate. Even in the white dwarf case, nuclear processes may be somewhat more important than the electron component which we treat here.

3.1 Electron-*s*electron scattering

In this work we treat the simplest of the above components, namely the conversion of electron to *s*electron pairs [28]:

$$e^-(p_1)e^-(p_2) \to \tilde{e}^-(p_3)\tilde{e}^-(p_4). \tag{3.1}$$

This cross section was calculated previously in [29] neglecting the electron mass as appropriate in the broken SUSY phase where the electron mass is many orders of

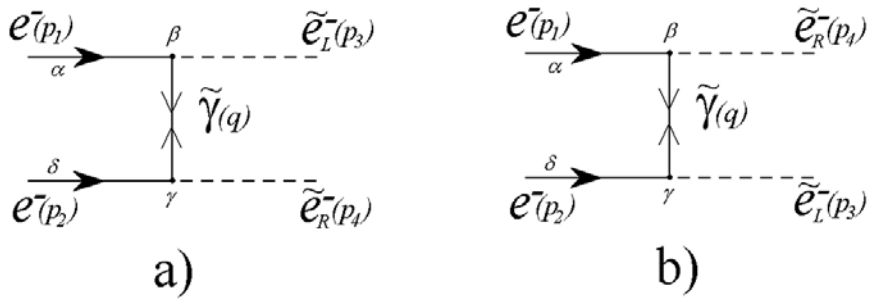

Figure 3.1: Feynman graphs for the conversion of an electron pair to *s*electrons via photino exchange

magnitude less than the *s*electron mass. In the exact SUSY phase the electron and *s*electron masses are equal and the cross section near threshold is needed.

We assume that the entire kinetic energy of the *s*electrons is released into gamma radiation as the scalars drop into the ground state although we do not treat the radiative processes explicitly.

In the process $e^-e^- \rightarrow \tilde{e}^-\tilde{e}^-$ the mediator of the interaction is a Majorana spinor $\tilde{\gamma}$ as shown in Figure 3.1.

For the associated production of left and right *s*electrons, the amplitudes corresponding to graphs *a* and *b* in Figure 3.1 are then

$$\begin{aligned} M_a &= \frac{\mathbf{i}e^2}{2(t-M_{\tilde{\gamma}}^2)} u^T(p_1)(1+\gamma_5)^T C^{-1}(\not{p}_1 - \not{p}_3 + M_{\tilde{\gamma}})(1-\gamma_5)u(p_2) \\ M_b &= \frac{\mathbf{i}e^2}{2(u-M_{\tilde{\gamma}}^2)} u^T(p_1)(1-\gamma_5)^T C^{-1}(\not{p}_1 - \not{p}_4 + M_{\tilde{\gamma}})(1+\gamma_5)u(p_2). \end{aligned}$$

Here and further the Mandelstam variables are

$$\begin{aligned} s &= (p_1+p_2)^2 \\ t &= (p_1-p_3)^2 \\ u &= (p_1-p_4)^2. \end{aligned}$$

So for calculating the matrix elements $|\mathcal{M}_{LR}|^2 = \Sigma_{ss'}\left(M_a M_a^\dagger + M_b M_b^\dagger + M_a M_b^\dagger + M_b M_a^\dagger\right)$

$$\begin{aligned} M_a M_a^\dagger &= \frac{e^2}{4(t-M_{\tilde{\gamma}}^2)^2} u^T(p_1)(1+\gamma_5)^T(\not{p}_1 - \not{p}_3 + M_{\tilde{\gamma}})^T \left(C^{-1}(1+\gamma_5)\right) u(p_2) \times \\ &\quad u^\dagger(p_2)\left(C^{-1}(1+\gamma_5)\right)^\dagger (\not{p}_1 - \not{p}_3 + M_{\tilde{\gamma}})^*(1+\gamma_5)^* u^*(p_1) = \\ &= \frac{e^2}{4(t-M_{\tilde{\gamma}}^2)^2} \left((\not{p}_1 + m_e)\gamma_0\right)^* (1+\gamma_5)^T(\not{p}_1 - \not{p}_3 + M_{\tilde{\gamma}})^T \times \\ &\quad \underbrace{\left(C^{-1}(1+\gamma_5)\right)(\not{p}_2 + m_e)\gamma_0\left(C^{-1}(1+\gamma_5)\right)^\dagger}_{\mathcal{A}} (\not{p}_1 - \not{p}_3 + M_{\tilde{\gamma}})^*(1+\gamma_5)^* \end{aligned}$$

$$\begin{aligned} \mathcal{A} &= C^{-1}(1+\gamma_5)(\not{p}_2 + m_e)\gamma_0(1+\gamma_5)^\dagger C \\ &= -C^{-1}(1+\gamma_5)(\not{p}_2 + m_e)C\gamma_0(1+\gamma_5) \\ &= -(1+\gamma_5)(-p_2 + m_e)^T\gamma^0(1+\gamma_5) \end{aligned}$$

$$
\begin{aligned}
M_a M_a^\dagger &= \frac{e^4}{4(t-M_{\tilde{\gamma}}^2)^2}(\not{p}_1+m_e)^*\gamma_0(1+\gamma_5)(\not{p}_1-\not{p}_3+M_{\tilde{\gamma}})^T(1+\gamma_5)(\not{p}_2-m_e)^T\times \\
&\quad \gamma_0(1+\gamma_5)(\not{p}_1-\not{p}_3+M_{\tilde{\gamma}})^*(1+\gamma_5)= \\
&= \frac{e^4}{4(t-M_{\tilde{\gamma}}^2)^2}(\not{p}_1+m_e)(1-\gamma_5)(\not{p}_1-\not{p}_3+M_{\tilde{\gamma}})(1-\gamma_5)(\not{p}_2-m_e)\times \\
&\quad (1+\gamma_5)(\not{p}_1-\not{p}_3+M_{\tilde{\gamma}})(1+\gamma_5) \\
&= \frac{e^4}{4(t-M_{\tilde{\gamma}}^2)^2}(-2\not{p}_1)(1-\gamma_5)(\not{p}_1-\not{p}_3+M_{\tilde{\gamma}})(-2\not{p}_2)(1+\gamma_5)(\not{p}_1-\not{p}_3+M_{\tilde{\gamma}}) \\
&= \frac{2e^4M_{\tilde{\gamma}}}{(t-M_{\tilde{\gamma}}^2)^2}\not{p}_1(1-\gamma_5)\not{p}_2(\not{p}_1-\not{p}_3+M_{\tilde{\gamma}}) = \frac{2e^4\not{p}_1\not{p}_2M_{\tilde{\gamma}}}{(t-M_{\tilde{\gamma}}^2)^2} = \\
&= \frac{8e^4p_1\cdot p_2M_{\tilde{\gamma}}}{(t-M_{\tilde{\gamma}}^2)^2} = \frac{8e^4M_{\tilde{\gamma}}}{(t-M_{\tilde{\gamma}}^2)^2}\frac{s-2m_e^2}{2} = \frac{4e^4(s-2m_e^2)M_{\tilde{\gamma}}}{(t-M_{\tilde{\gamma}}^2)^2}
\end{aligned}
$$

$$
M_bM_b^\dagger = \frac{4e^4(s-2m_e^2)M_{\tilde{\gamma}}}{(u-M_{\tilde{\gamma}}^2)^2}
$$

$$
M_aM_b^\dagger = \frac{4e^4(s-2m_e^2)M_{\tilde{\gamma}}}{(u-M_{\tilde{\gamma}}^2)(t-M_{\tilde{\gamma}}^2)}
$$

The matrix elements take the form:

$$
\begin{aligned}
|\mathcal{M}_{LR}|^2 &= \Sigma_{ss'}\left(M_aM_a^\dagger+M_bM_b^\dagger+M_aM_b^\dagger+M_bM_a^\dagger\right) \\
&= e^4\left[\frac{1}{(t-M_{\tilde{\gamma}}^2)^2}\left(ut-2tm_e^2-\left(m_{\tilde{e}}^2-m_e^2\right)^2\right)\right. \\
&\qquad \left. +\,t\leftrightarrow u+\frac{4m_e^2\left(m_{\tilde{e}}^2-m_e^2\right)}{(t-M_{\tilde{\gamma}}^2)(u-M_{\tilde{\gamma}}^2)}\right] \qquad (3.2)
\end{aligned}
$$

where $\Sigma_{ss'}$ denotes averaging over the spins of incoming particles. The production of two left or two right $s$electrons is obtained from the above by the appropriate changes in the helicity projection operators and dividing by the statistical factor for

the identical final state particles.

$$|\mathcal{M}_{RR}|^2 = |\mathcal{M}_{LL}|^2 = \frac{e^4 M_{\tilde{\gamma}}^2}{2!}\left(s - 2m_e^2\right)\left(\frac{1}{t - M_{\tilde{\gamma}}^2} + \frac{1}{u - M_{\tilde{\gamma}}^2}\right)^2. \tag{3.3}$$

In the limit of negligible electron mass, these agree with the spin-averaged formulae of [30] and with the squared helicity amplitudes of [29]. Other authors have considered the effect of other neutralino exchanges [31, 32] but, since these particles in the SUSY phase have masses comparable to the W and Z, they are negligible for our purposes.

In the numerical simulations we will need the integrated matrix elements squared:

$$f_{AB}(s) = \frac{1}{\sqrt{s(s-4m^2)}}\int_{4m^2-s}^{0} dt|\mathcal{M}_{AB}|^2. \tag{3.4}$$

The total cross sections are related to the f_{AB} by

$$\sigma_T(ee \to \tilde{e}_A\tilde{e}_B) = \frac{f_{AB}(s)}{16\pi\sqrt{s(s-4m^2)}}. \tag{3.5}$$

Calculations for the different Matrix elements in the SUSY phase ($m_e = m_{\tilde{e}} = m$) will give us the following:

$$\begin{aligned}
f_{LR}(s) &= 2e^4\sqrt{\frac{s-4m^2}{s}}\left(\frac{-2s - 2M_{\tilde{\gamma}}^2 + 6m^2}{s - 4m^2 + M_{\tilde{\gamma}}^2} + \frac{s - 2m^2 + 2M_{\tilde{\gamma}}^2}{s-4m^2}\ln\frac{s - 4m^2 + M_{\tilde{\gamma}}^2}{M_{\tilde{\gamma}}^2}\right) \\
f_{LL}(s) &= f_{RR}(s) = \\
&= \frac{4e^4(s-2m^2)}{\sqrt{s(s-4m^2)}}\left(\frac{s-4m^2}{(s-4m^2+M_{\tilde{\gamma}}^2)} + \frac{2M_{\tilde{\gamma}}^2}{s-4m^2+2M_{\tilde{\gamma}}^2}\ln\frac{s-4m^2+M_{\tilde{\gamma}}^2}{M_{\tilde{\gamma}}^2}\right).
\end{aligned}$$

These are only logarithmically sensitive to the photino mass. The *s*electron mo-

mentum and angular distributions to be calculated in the next section are even less sensitive to the photino mass since they depend only on the shape of the cross sections and not on the absolute values. Integrals of f_{LL} and f_{LR} as required in the conversion rates discussed in the next section are finite in the limit of zero photino mass.

3.2 Event generation

In a typical white dwarf (solar mass and Earth radius) there are $N_0 = 6 \cdot 10^{56}$ electrons in a degenerate Fermi sea:

$$dN = \frac{2p^2 dp\, d(\cos\theta)\, d\phi}{(2\pi\hbar)^3}. \tag{3.6}$$

The Fermi momentum is

$$p_{max} = \left(\frac{3N}{8\pi V}\right)^{1/3} 2\pi\hbar = 0.498 MeV/c. \tag{3.7}$$

The event rate for process (3.1) in a volume V is given in terms of the differential cross section by

$$\Gamma = \int d\sigma \left(\frac{dN_i v_i}{V}\right) dN_t. \tag{3.8}$$

where the incident and target distributions are given by (3.6). The differential cross section is given in terms of the invariant matrix element squared by

$$d\sigma = \frac{\mid \mathcal{M} \mid^2 d\Omega_f}{4E_1 E_2 v}. \tag{3.9}$$

Here m is the common electron and $s$electron mass in the SUSY bubble. The final

state phase space is

$$d\Omega_f = \frac{d^3p_3}{2E_3}\frac{d^3p_4}{2E_4}\frac{\delta^4(p_1+p_2-p_3-p_4)}{(2\pi)^2} \tag{3.10}$$

where any statistical factors that occur for identical final state particles are put into the matrix element squared. Thus the Lorentz invariant event rate per unit volume is

$$\frac{d\Gamma}{V} = \frac{4|\ \mathcal{M}\ |^2}{(2\pi)^8}\frac{d^3p_1}{2E_1}\frac{d^3p_2}{2E_2}\frac{d^3p_3}{2E_3}\frac{d^3p_4}{2E_4}\delta^4(p_1+p_2-p_3-p_4). \tag{3.11}$$

The p_2 integral can be done trivially using the δ function and the p_1 integral is then conveniently done in the CM frame with $\hat{p}_3 = \hat{e}_z$.

$$\frac{d^3p_1}{2E_1}\delta((p_3+p_4-p_1)^2-m^2) = \frac{\pi dt}{2\sqrt{s(s-4m^2)}}. \tag{3.12}$$

Thus

$$\frac{d\Gamma}{V} = \frac{|\ \mathcal{M}\ |^2}{(2\pi)^7\sqrt{s(s-4m^2)}}dt\frac{d^3p_3}{2E_3}\frac{d^3p_4}{2E_4}. \tag{3.13}$$

or

$$\frac{d\Gamma}{V} = \frac{|\ \mathcal{M}\ |^2}{(2\pi)^7\sqrt{s(s-4m^2)}}dt\frac{{p_3}^2}{2E_3}\frac{{p_4}^2}{2E_4}dp_3\, d\cos\theta_3\, d\phi_3 dp_4 d\cos\theta_4\, d\phi_4. \tag{3.14}$$

For p_{max} we use the value of (3.7) corresponding to the Fermi energy in a white dwarf of earth radius and solar mass.

The final state of the process consists of two distinct species of scalars, $\tilde{e}_L$ and $\tilde{e}_R$.

Thus the effective matrix element squared in (3.14) and elsewhere above is actually

$$\mid \mathcal{M} \mid^2 = \mid \mathcal{M}_{LR} \mid^2 + (\mid \mathcal{M}_{LL} \mid^2 + \mid \mathcal{M}_{RR} \mid^2) \tag{3.15}$$

In a bath of pre-existing $s$electrons each matrix element squared is related to the elementary matrix element squared calculated with no pre-existing $s$electrons by the Bose statistical factors

$$\begin{aligned} \mid \mathcal{M} \mid^2 &= \mid \mathcal{M}_{0_{LR}} \mid^2 (N_L(\vec{p}_3)+1)(N_R(\vec{p}_4)+1) + (\mid \mathcal{M}_{0_{LL}} \mid^2 (N_L(\vec{p}_3)+1)(N_L(\vec{p}_4)+1) \\ &+ \mid \mathcal{M}_{0_{RR}} \mid^2 (N_R(\vec{p}_3)+1)(N_R(\vec{p}_4)+1)). \end{aligned} \tag{3.16}$$

The matrix elements of the previous section, calculated for the case of no $s$electrons in the initial state, are the $\mathcal{M}_0$ of this section. For the present we treat only the LL final state. The RR final state implies that there will be at least four gamma ray jets in each burst and possibly many more if multiple SUSY bubbles are nucleated in a star and different energy levels in the Fermi sea lead to independent gamma ray bursts. This suggests a picture where the gamma ray jets are much more numerous in each stellar explosion and, individually, much more narrow and less energetic than currently assumed.

Our remaining analysis, restricted to the LL jets, allows us to drop, the L subscript on the occupation numbers. The CM energy $\sqrt{s}$ is determined by $\vec{p}_3$ and $\vec{p}_4$.

We define a grid of N_{bin} points in each of the six variables. In practice we choose

$N_{bin} = 10$. The discretized $i'th$ integration variable in (3.14) is

$$v_i = v_{i,min} + (v_{i,max} - v_{i,min})(N_i + 1/2)/N_{bin} \tag{3.17}$$

where $0 \leq N_i \leq N_{bin} - 1$. In order to generate events with probability defined by (3.14) and (3.16), it is convenient to linearize the six dimensional integral. We define the composite integer variable

$$j = \sum_{i=1}^{6} N_{bin}^{6-i} N_i \tag{3.18}$$

with limits

$$0 \leq j \leq N_{bin}^6 - 1. \tag{3.19}$$

Each value of j corresponds to a unique value of each of the six integration variables. The distribution of events is then defined as an integer valued array with N_{bin}^6 grid points. To handle 10^6 grid points requires careful memory management techniques. [1] The integer j can be decomposed into two integers j_3 and j_4 which encode the three dimensional vectors $\vec{p_3}$ and $\vec{p_4}$ respectively.

$$\begin{aligned} j_3 &= j/N_{bin}^3 \\ j_4 &= j \bmod N_{bin}^3 \\ j &= N_{bin}^3 j_3 + j_4. \end{aligned} \tag{3.20}$$

[1] We thank Doug Leonard for consultation on these techniques.

The first of these equations is defined by integer division, i.e. j_3 is the largest integer less than or equal to j/N_{bin}^3. The event generation follows standard techniques [33] except that the probability distribution changes with each event due to the Bose enhancement factors. In the event generation of the *s*electron distributions, constant overall factors in (3.14) play no role. We begin by putting all the *s*electron occupation numbers to zero and calculating the (unnormalized) probabilities

$$P(j) = f_{LL}(s)\frac{p_3^2 p_4^2}{E_3 E_4}(N(j_3)+1)(N(j_4)+1). \tag{3.21}$$

We then define the partial sum

$$R(j) = \sum_{i=0}^{j} P(i) \tag{3.22}$$

as well as the complete sum

$$P_{int} = \sum_{i=0}^{N_{bin}^6-1} P(i). \tag{3.23}$$

$R(j)$ is a monotonically increasing function of j. One then calls a random number w between zero and one. For the unique value of j for which $w > R(j-1)/P_{int}$ and $w \leq R(j)/P_{int}$ one increments the *s*electron occupation numbers by one:

$$\begin{aligned} N(j_3) &\rightarrow N(j_3)+1 \\ N(j_4) &\rightarrow N(j_4)+1 \end{aligned} \tag{3.24}$$

$P(j\prime)$ changes in the jth bin only by a factor

$$f = (N(j_3) + 1)(N(j_4) + 1)/(N(j_3)N(j_4)). \tag{3.25}$$

Here $N(j_3)$ and $N(j_4)$ are the new occupation numbers (after incrementing). $R(j\prime)$ changes for each $j\prime \geq j$

$$R(j\prime) \rightarrow R(j\prime) + P(j)(f-1) \qquad for \qquad j\prime \geq j. \tag{3.26}$$

In addition

$$P_{int} \rightarrow P_{int} + P(j)(f-1). \tag{3.27}$$

After making these replacements, one adjusts $P(j)$:

$$P(j) \rightarrow P(j)f. \tag{3.28}$$

One then repeats the process as many times as possible choosing new random values of w. After very many events the distribution is amplified at two particular values of $\vec{p_3}$ and $\vec{p_4}$.

In the simulation two problems arise. The first is that the enhanced probability to put subsequent events in some particular $j'th$ bin is a very mild enhancement at first. Only after some huge number of events does the structure lock in on a particular j value. Since the number of available fermions in a compact star is of order 10^{56}, this is not a problem in principle but it obviously pose some technical

p (MeV)	N(p)	$\cos\theta$	N($\cos\theta$)	ϕ	N(ϕ)
0.017	42	-0.93	60914	$2/15\,\pi$	16692
0.050	360	-0.80	87034	$4/15\,\pi$	56060
0.083	986	-0.67	41284	$6/15\,\pi$	94394
0.116	1948	-0.53	28832	$8/15\,\pi$	30174
0.149	3178	-0.40	14672	$10/15\,\pi$	63792
0.183	4690	-0.27	24064	$12/15\,\pi$	127048
0.216	6572	-0.13	16452	$14/15\,\pi$	607026
0.249	8410	0.00	52874	$16/15\,\pi$	13538
0.282	11510	0.13	660320	$18/15\,\pi$	50778
0.315	13548	0.27	16302	$20/15\,\pi$	21316
0.349	17198	0.40	33942	$22/15\,\pi$	46504
0.382	26284	0.53	112400	$24/15\,\pi$	25394
0.415	63298	0.67	23458	$26/15\,\pi$	13670
0.448	82526	0.80	23878	$28/15\,\pi$	31868
0.481	1034494	0.93	78618	$2\,\pi$	76790

Table 3.1: *S*electron momentum and angular distributions showing the effect of boson enhancement. In this run the occupation numbers are incremented by two at each throw of the dice

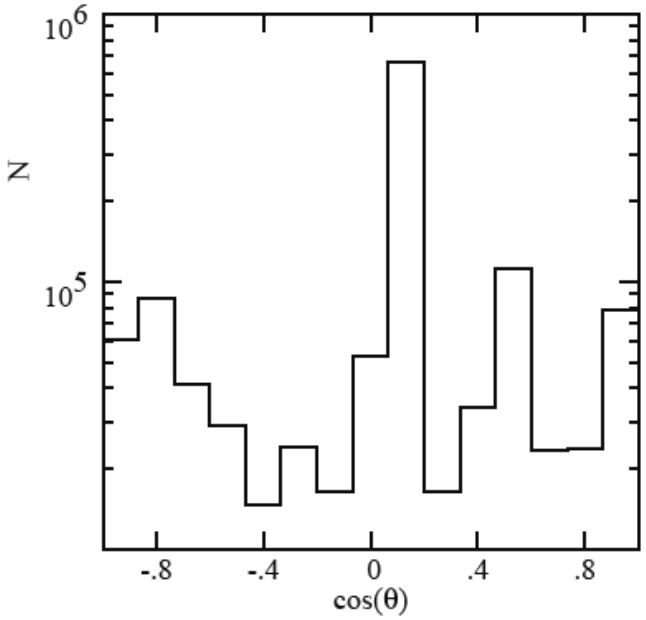

Figure 3.2: Angular distribution after $6 \cdot 10^5$ throws, showing effect of Bose enhancement. In this run the bins are incremented twice at each throw.

problems. To accelerate the buildup of jet structure, instead of incrementing the *s*electron occupation numbers by one at each throw of the dice, we increment by two. In a simplified run where we look at the conversion of two electrons at the Fermi surface, although there are no observable jets in the first million events, a clear jet structure emerges at $9 \cdot 10^7$ events even when *s*electron occupation numbers are incremented by one at each event as is physically required.

If one increments by more than one at each throw, the f of (3.25) has to be redefined accordingly. The distributions in *s*electron momentum, polar angle cosine, and azimuthal angle after $600,000$ throws is shown in Table 3.2. The polar distribution of these simulations are presented in the Figure 3.2

The second problem is the following. We have treated the star as having an inexhaustible supply of electrons of each momentum in the Fermi sea. In practice this number is very large but not infinite. Only after all the electrons have been

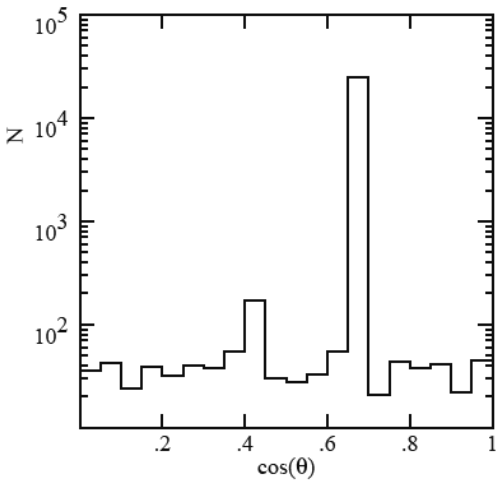

Figure 3.3: Polar angle distribution for conversion of those electron pairs whose center of momentum is that of the star. One quadrant of the angular space is shown with a balancing *s*electron jet in the opposite direction.

exhausted will the *s*electron momenta add to zero in the rest frame of the star. For the present we circumvent this problem by considering electron to *s*electron conversion among those electron pairs whose center of momentum frame is that of the star. Then we can choose one *s*electron according to the distribution of (3.14) with the other *s*electron necessarily having the balancing momentum. In this case we can see rapid jet structure development. The corresponding *s*electron distribution is shown in Figure 3.3 after only 50,000 events.

Chapter 4

Nuclear Calculations

In a previous chapter we considered a SUSY transition in a pair of $ee \rightarrow \tilde{e}\tilde{e}$. This transition includes the electrons atoms. A very similar transition will occur inside the nucleus of each atom. For example, each carbon-12 nucleus contains $(6 + 6) \times 3 = 36$ quarks, that will undergo SUSY transition. Calculating the amplitudes for this process is one of the future goals in the development of this model.

Nevertheless, one can consider collective models for the nuclei to include the nucleons' transition into the total energy release. In this work, three of the most developed models are used. Energy outputs for all of them including nuclear transitions and possible nuclear fusion are calculated.

4.1 Nuclear models

4.1.1 Liquid Drop model

The behavior of drops of liquid can be a good analogy for the description of nuclei. Such a model will be purely empirical and will require fitting parameters, which are measured experimentally. There were several attempts to use such a model, the most

successful one is known as a Weizsaecker's formula for the total nuclear energy[34].

The construction of this formula is straightforward. The total energy can be calculated as the total mass of nucleons $Zm_p + Nm_n$ (here $m_p,\ Z$ - mass and number of protons, $m_n,\ N$ - mass and number of neutrons) minus the total binding energy. One just needs to express the total binding energy through $Z,\ N,\ A = Z + N$. The first term in the binding energy should be proportional to the total volume of the nucleus, which is proportional to the total number of nucleons. Therefore the volume term will be $E_V = a_V A$. From here one can also see that radius of the nucleus will be proportional to $A^{1/3}$.

The nucleons that are close to the surface of the drop have fewer neighbors, and, as a consequence, the total binding energy will be reduced by a value proportional to the surface area (square of the radius) expressed as $a_S A^{2/3}$. The Coulomb repulsion of the protons inside the nuclei can be effectively described as an interaction of Z protons with the remaining core of $Z - 1$ protons on distances of roughly the size of the nuclei thus inversely proportional to the radius of the nuclei $a_C Z(Z-1)A^{-1/3}$. The Pauli principle favors nuclei with $A = 2Z$, so the empirical formula has a fourth (asymmetry) term with coefficient of a_A. The Pauli principle also favors nuclear configurations with even numbers of neutrons and protons. In the liquid drop model, this is included by using the even-odd nucleus as a reference and adding a correction term to the binding energy which is positive for even-even nuclei and negative for odd-odd nuclei. This is δ in the formula. Different parameter fits use a different dependence on A of the δ-term. Most used ones have $A^{-3/4}$ and $A^{-1/2}$ proportionality.

According to this model the total binding energy of the nuclei is described by this

	1	2	3	4	5
a_V	15.67	15.5	14.1	15.75	15.8
a_S	17.23	16.8	13	17.8	18.3
a_C	0.714	.72	.595	.711	.714
a_A	93.15	23	19	23.7	23.2
n	-1/2	$-3/4$	0	-1/2	-1/2
δ	11.5	34	33.5	11.8	12

Table 4.1: Parameter sets for liquid drop model of nuclei

equation:

$$E_{\mathrm{B}} = a_V A - a_S A^{2/3} - a_C Z(Z-1)A^{-1/3} - a_A \frac{(A-2Z)^2}{A} + \delta(A,Z)A^n \qquad (4.1)$$

The most commonly used parameters of this equation are given in Table 4.1. Results of total nuclear energy calculations are given in Table 4.2. Here and later the parameter sets are referred as follows:

1. Average accepted set
2. by Krane[34]
3. by Wapstra[35]
4. Rohlf[36]
5. Least-square fit for accepted nuclear masses [37]

If the SUSY transition occurs, then in the first order approximation, nucleons

will convert into their supersymmetric partners and will lose any fermionic behavior. Hence, all terms in this formula associated with the Pauli principle will disappear.

Although the liquid drop model works fine for the binding energies for most nuclei (especially with $A > 14$), it is purely empirical and does not give an explanation for any periodical properties of the nuclei (similar to the periodical structure of the elements) and the existence of so-called "magic numbers". The shell model of nuclei gives some understanding of this phenomena.

Nucleus	1	2	3	4	5	Experiment
^{3}He	2850.71	2813.22	2808.01	2814.77	2815.50	2808.29
^{4}He	3731.57	3724.90	3699.29	3732.84	3733.49	3727.24
^{7}Li	6554.14	6531.61	6526.54	6533.59	6535.01	6533.60
^{7}Be	6555.08	6532.57	6527.11	6534.52	6535.95	6533.95
^{8}Be	7455.14	7451.73	7420.63	7456.87	7458.20	7454.58
^{8}B	7557.98	7479.11	7498.21	7478.17	7479.84	7472.05
^{12}C	11175.35	11173.26	11140.28	11177.43	11179.25	11174.46
^{13}C	12124.12	12108.95	12104.24	12111.17	12113.28	12109.04
^{13}N	12126.46	12111.32	12105.97	12113.50	12115.62	12110.75
^{14}N	13041.10	13042.71	13066.86	13043.15	13045.63	13039.73
^{15}N	13981.67	13967.93	13963.42	13970.15	13972.46	13968.43
^{15}O	13984.42	13970.71	13965.50	13872.89	13975.21	13970.67
^{16}O	14894.40	14893.14	14859.39	14896.75	14898.99	14894.54
^{20}Ne	18613.05	18612.46	18578.41	18615.63	18618.23	18617.06
^{23}Na	21413.88	21404.03	21400.49	21406.05	21409.04	21408.44
^{23}Mg	21418.11	21408.30	21403.79	21410.25	21413.26	21411.99
^{24}Mg	22331.69	22331.67	22297.57	22334.44	22337.37	22334.99
^{28}Si	26050.50	26051.03	26016.99	26053.39	26056.63	26052.25
^{31}P	28848.60	28841.33	28838.75	28842.87	28846.44	28843.17
^{31}S	28854.12	28846.91	28843.13	28848.36	28851.96	28848.06
^{32}S	29769.61	29770.67	29736.75	29772.62	29776.15	29772.55
^{36}Ar	33489.11	33490.70	33456.90	33492.22	33496.01	33493.15
^{48}Cr	44650.36	44653.54	44619.93	44653.64	44658.18	44642.28
^{56}Fe	52178.39	52087.26	52055.82	52086.74	52091.51	52087.90
^{56}Ni	52093.75	52098.04	52064.28	52097.06	52102.07	52093.58
^{60}Zn	55816.26	55821.11	55787.17	55819.57	55824.79	55818.12

Table 4.2: Total nuclear energies (in MeV) for different sets of parameters

4.1.2 Shell model

It is found that nuclei with even numbers of protons and neutrons are more stable than those with odd numbers. In particular, there are "magic numbers" of neutrons and protons which seem to be particularly favored in terms of nuclear stability: 2, 8, 20, 28, 50, 82, 126. Surely one would hope to find the model similar to a shell model of atoms.

In the shell model, nucleons are considered as particles bound in a potential with the characteristic size of the nuclear diameter. The problem becomes a straightforward quantum mechanical system. Solving it will get the energy levels for the nucleons inside the mentioned potential. For different forms of the potential the structure of the energy levels will have slight corrections but the overall behavior remains the same. Nuclei exhibit a shell structure similar to one for the Bohr model of the atom. Fine tuning of the potential will allow us to create the most realistic model.

To start we will choose the simplest shell model - the simple rectangular 3-dimensional well:

$$V = \begin{cases} -V_0 & \text{for} \quad r < R \\ 0 & \text{for} \quad r > R \end{cases}$$

One should note that the protons and neutrons are filling their own wells. As calculations show, the results are quite satisfactory for the fermionic-type nuclei. For the model for bosonic-types we will populate just the lowest level of energy for the same potentials. This becomes possible due to the fact that the nucleons are bosons, hence do not obey the Pauli exclusion. The results of this are used as a next order approxi-

mation for the nuclear fusion energy calculations and discussed in the "Calculations" section of this chapter.

A more realistic form of the well potential will take into account Coulomb repulsion of the protons. This is the major difference in the nucleons' potentials that can nicely explain the abundance of the neutrons in stable heavy nuclei. In order for the nucleus to be stable the top filled levels for both potentials need to be the same. But since the bottom of the protons' potential is higher than neutrons' one - the number of filled levels for neutrons is larger.

One should also consider a more realistic shape of the potential

$$V(r) = \frac{-V_0}{1 + \exp\left[\frac{r-R}{a}\right]}$$

The solution for the energy levels for such a potential creates the set of magic numbers for totally filled nucleon shells. However this set is a bit different from the observed one: 2, 8, 18, 20, 34, 40, 58,... This issue could be resolved by adding a non-central term to the potential. In the nucleus, nucleons are tightly packed into a small volume which makes the introduction of spin-orbital interaction very sensible. The perturbation of the central potential with

$$\Delta V = V_1 \overrightarrow{L} \cdot \overrightarrow{S}$$

where V_1 is negative, gives the right energy level splitting and produces the right set of magic numbers: 2, 8, 20, 28, 50, 82, 126. In our work we will also consider this

model for the nuclei. During the phase transition to the SUSY state, the whole tower of nucleons held on upper levels inside the potential will spontaneously collapse to the lower level, since it is no longer supported by the Pauli exclusion principle. More consideration of the effects of the SUSY transition is given in the discussion about the computational results in this chapter.

4.1.3 Fermi gas model

Both models considered above give satisfactory results for the total energy of the nucleus calculations. One may argue that these models heavily depend on empirical parameters which are determined by experimental data. This is an absolutely valid remark. As we said before these models can be used as zeroth order approximations for the nuclear calculations.

Now the question is - is there an *ab-initio* model for the nuclei that gives any satisfactory results which one can generalize to bosonic nuclei? As a matter of fact, in the Fermi Gas model nuclei possess some of these qualities.

In this model nucleons are considered to be quasi-free within the volume of the nucleus. The binding potential is created by all nucleons. Each type of nucleon fills its own potential well.

Neglecting the spin, the total number of states for each nucleon type is given by

$$\mathrm{d}n = \frac{4\pi p^2 \mathrm{d}p}{(2\pi\hbar)^3} V \qquad \Rightarrow \qquad n = \frac{p_F^3}{6\pi^2\hbar^3} V$$

where

$$V = \frac{4}{3}\pi R_0^3 A, \quad R_0 = 1.2\,\mathrm{fm}.$$

Here, R_0 is again an empirical parameter. For the fermionic-type nucleons it is fixed to the above value. For the bosonic type nucleons, this instead can be taken as a variational parameter for finding the minimum for the total energy.

In the Fermi gas, according to the Pauli exclusion principle, each state can be filled with two nucleons. So the total number of neutrons and protons can be expressed as

$$N = \frac{p_{Fn}^3}{3\pi^2\hbar^3}V, \quad Z = \frac{p_{Fp}^3}{3\pi^2\hbar^3}V.$$

In the case of a symmetric nucleus $Z = N = A/2$ the magnitude of the Fermi momentum can be easily calculated:

$$p_F = p_{Fn} = p_{Fp} = \frac{\hbar}{R_0}\left(\frac{9\pi}{8}\right)^{1/3} \approx 250\,\mathrm{MeV}/c.$$

The Fermi energy corresponding to highest occupied nucleon level is

$$E_F = \frac{p_F^2}{2m_N} \approx 33\,\mathrm{MeV}.$$

The difference between the edge of the potential well and the top filled level should be the average binding energy per nucleon (7-8 MeV). So the depth of the potential well is around 40 MeV.

Including the Coulomb repulsion into consideration will lead to asymmetry in Z

and N. First, the Fermi level for protons and neutrons has to be the same, otherwise the nucleus would decay into a more energetically favorable state via β-decay. This leads to a difference in occupancy of the levels for protons and neutrons. Neutrons gain extra levels at the bottom of the potential well and as consequence, the nuclei with neutron abundance become more stable.

Inside the nucleus, neutrons and protons are in the ground state so kinetic energy can be treated as an anti-binding energy. Weizsaecker's formula gives corrections to the total energy for a nucleus with different numbers for protons and neutrons. Since both models give satisfactory results for the total nuclear energy, coefficients of Weizsaeker's formula can be derived from the Fermi gas model. One needs to find the dependence of the total nuclear energy on the total number of protons, Z, the total number of neutrons, N, or any combination.

A numerical description of the energy dependance on $Z - N$ could be shown as the following:

$$\langle E_{kin} \rangle = \frac{\int_0^{p_F} E_{kin} p^2 \mathrm{d}p}{\int_0^{p_F} p^2 \mathrm{d}p} = \frac{3}{5} \frac{p_F^2}{2m_N} \approx 20\mathrm{MeV}$$

The total kinetic energy of the nucleus can be then described as

$$\begin{aligned} E_{kin}(N,Z) &= N\langle E_{kin}^{\{n\}} \rangle + Z\langle E_{kin}^{\{p\}} \rangle = \frac{3}{10m_N}(Np_{Fn}^2 + Zp_{Fp}^2) = \\ &= \frac{3}{10m_N} \frac{\hbar^2}{R_0^2} \left(\frac{9\pi}{4}\right)^{2/3} \frac{N^{5/3} + Z^{5/3}}{A^{2/3}}. \end{aligned}$$

Taking $A = Z + N$ and expanding in $N - Z$ one can get

$$E_{kin}(N,Z) = \frac{3}{10m_N}\frac{\hbar^2}{R_0^2}\left(\frac{9\pi}{8}\right)^{2/3}\left(A + \frac{5}{9}\frac{(N-Z)^2}{A} + ...\right). \tag{4.2}$$

The first term is a negative correction to the volume term in Weizsaecker's formula, the second is an asymmetry term. As in the liquid drop model, the volume term in the Fermi gas model is leading in magnitude.

The asymmetry term is $\frac{1}{6}\left(\frac{9\pi}{8}\right)^{2/3}\frac{\hbar^2}{m_N R_0^2}\frac{(N-Z)^2}{A}$ and has the coefficient $a_A^{\text{Fermi}} = 11.09\,MeV$ which is close to most Weizsaecker's formula fits. The volume term $\frac{3}{10m_N}\frac{\hbar^2}{R_0^2}\left(\frac{9\pi}{8}\right)^{2/3}A$ with coefficient $a_V^{\text{Fermi}} = 19.97\,MeV$ has a different sign and value. This should not be surprising, since the two formulae are using different zeroth energy. In the Fermi gas model, the volume correction to the energy is added to the total energy of nucleons in a confined state. In the liquid drop model, the volume correction term is decreasing the energy from the total energy of free nucleons.

4.2 Calculations

The purpose of considering the nuclear models was to calculating the energy output during the SUSY transition. In our work we used all of the above models to calculate the energies.

During the transition into a supersymmetric state, all of the fermions become bosons. It is reasonable to assume that all of the constants, describing the collective behavior, remain the same for a brief time, at least. During this time, the only part of the inherited behavior which will be "turned off" is the part that is caused by the

Pauli exclusion principle.

We will start our discussion of energy release with consideration of Weizsaeker's formula. The only correction to the formula for the supersymmetric state will be equating the terms a_A to zero and δ to the smallest possible value, since $-\delta$ corresponds to the lowest energy state. Since for most of the atoms both coefficients are negative this will lead to a positive difference in total mass, hence to energy release during transition into a supersymmetric state. The results of calculations of the total nuclei energy release are given in Table 4.3. For different sets of parameters the resultant total energy of the nuclei is smaller than for ordinary matter. This means that during the SUSY transition the average nucleus is releasing energy in the amount of 5 MeV per nucleus. This is equivalent to 3.69×10^{59} MeV or 5.91×10^{53} erg of total energy[1].

Besides the energy release for the individual nuclei, the transition into a new phase opens the possibility for nuclear fusion reactions that were forbidden before, due to energy conservation. As one can see from Table 4.4, nuclear fusion reactions become more energetic in the SUSY state, which leads to additional energy release of 61.2 MeV per final Zn atom or 4.53×10^{57} MeV (2.91×10^{51} erg) per star. Surely the process of nuclear fusion may go further, but we are considering only first stages of the fusion since after the transition the collective models for the nuclei may change their parameters with time.

Summarizing the effects of SUSY transitions calculated for different parameters

[1]Here and later we are using characteristic parameters for white dwarfs: mass of Sun and size of Earth.

Nucleus	1	2	3	4	5	Shell model	Fermi gas
^{4}He	0.00	0.00	0.00	0.00	0.00	0.0	0.0
^{7}Li	29.80	11.19	36.21	7.61	7.85	3.08	71.00
^{7}Be	29.80	11.19	36.21	7.61	7.85	3.08	71.02
^{8}Be	0.00	0.00	0.00	0.00	0.00	3.76	80.25
^{8}B	101.28	25.80	76.50	19.76	20.09	3.76	83.06
^{12}C	0.00	0.00	0.00	0.00	0.00	5.73	120.37
^{13}C	20.04	6.74	34.96	4.92	5.11	6.11	130.82
^{13}N	20.04	6.74	34.96	4.92	5.11	6.11	130.84
^{14}N	6.15	9.40	67.00	5.98	6.41	6.47	140.43
^{15}N	18.28	5.99	34.77	4.47	4.65	6.79	150.82
^{15}O	18.28	5.99	34.77	4.47	4.65	6.79	150.84
^{16}O	0.00	0.00	0.00	0.00	0.00	7.10	160.49
^{20}Ne	0.00	0.00	0.00	0.00	0.00	10.72	267.48
^{23}Na	13.92	4.24	34.33	3.36	3.51	12.91	307.91
^{23}Mg	13.92	4.24	34.33	3.36	3.51	12.91	307.95
^{24}Mg	0.00	0.00	0.00	0.00	0.00	13.57	320.98
^{28}Si	0.00	0.00	0.00	0.00	0.00	15.92	374.48
^{31}P	11.50	3.33	34.11	2.77	2.90	17.45	414.82
^{31}S	11.50	3.33	34.11	2.77	2.90	17.45	414.86
^{32}S	0.00	0.00	0.00	0.00	0.00	17.93	427.97
^{36}Ar	0.00	0.00	0.00	0.00	0.00	19.68	481.47
^{48}Cr	0.00	0.00	0.00	0.00	0.00	28.08	722.21
^{56}Fe	101.82	6.57	5.43	6.77	6.63	33.08	844.89
^{56}Ni	0.00	0.00	0.00	0.00	0.00	33.08	842.58
^{60}Zn	0.00	0.00	0.00	0.00	0.00	35.29	902.76

Table 4.3: Total nuclear energy releases (in MeV) for different models and sets of parameters

Reaction	1	2	4	5	shell model	Fermi gas
$^{12}C + {}^{12}C \rightarrow {}^{24}Mg + \gamma$	19.01	14.84	20.42	21.14	6.06	80.25
$^{12}C + {}^{12}C \rightarrow {}^{23}Mg + n$	6.93	2.88	8.40	9.18	2.63	54.90
$^{12}C + {}^{12}C \rightarrow {}^{23}Na + p$	12.46	8.45	13.90	14.70	2.63	54.91
$^{12}C + {}^{12}C \rightarrow {}^{20}Ne + \alpha$	9.24	9.16	10.83	11.88	1.51	26.75
$^{12}C + {}^{12}C \rightarrow {}^{16}O + 2\alpha$	-0.50	3.57	1.31	2.72	-3.99	-80.25
$^{16}O + {}^{16}O \rightarrow {}^{32}S + \gamma$	19.18	15.61	20.87	21.82	6.67	106.99
$^{16}O + {}^{16}O \rightarrow {}^{31}S + n$	6.61	3.14	8.34	9.35	3.21	81.69
$^{16}O + {}^{16}O \rightarrow {}^{31}P + p$	13.43	10.02	15.13	16.17	3.21	81.70
$^{16}O + {}^{16}O \rightarrow {}^{28}Si + \alpha$	9.90	10.36	11.71	12.94	1.49	53.30
$^{16}O + {}^{16}O \rightarrow {}^{24}Mg + 2\alpha$	0.31	4.81	2.26	3.81	-3.65	0.00
$^{28}Si + {}^{28}Si \rightarrow {}^{56}Ni + \gamma$	7.24	4.02	9.72	11.19	8.04	93.62
$^{56}Ni \rightarrow {}^{56}Fe + 2e + 2\bar{\nu}$	16.16	16.33	16.08	16.16	-1.02	-1.79
$^{12}C + {}^{24}Mg \rightarrow {}^{36}Ar + \gamma$	17.93	14.24	19.65	20.61	6.70	100.31
$^{12}C + {}^{36}Ar \rightarrow {}^{48}Cr + \gamma$	14.10	10.41	16.01	17.08	7.00	60.18
$^{12}C + {}^{48}Cr \rightarrow {}^{60}Zn + \gamma$	9.45	5.69	11.50	12.64	7.19	60.18
$^{24}Mg + {}^{24}Mg \rightarrow {}^{48}Cr + \gamma$	13.01	9.80	15.24	16.56	7.64	80.25
$^{24}Mg + {}^{36}Ar \rightarrow {}^{60}Zn + \gamma$	4.53	1.26	7.08	8.58	8.13	40.12

Table 4.4: Nuclear fusion reactions and their energy outputs in SUSY state for different sets of parameters of liquid drop, shell and Fermi gas models (MeV)

of the liquid drop model, we can estimate the total energy output of 4.84×10^{57} MeV.

Similar calculations were performed for the shell model of the nuclei. In this case the major effect of the transition comes from the avalanche of nucleons stored in the Pauli tower. Similar to the first case scenario, the nuclei release energy during this transition. Additional energy release comes from nuclear synthesis due to the fact that nuclear fusion is no longer forbidden. Results of the calculations are presented in Table 4.4.

As one can observe the total energy output for the SUSY transition in this model is around 2.47×10^{57} MeV, which is in agreement with the models considered above.

Finally, the last approach we used for descibing the nuclei was the Fermi gas model. Since this model is the least parameterized it should give a more general result for the calculation of the total energy release.

Once again we calculated the total energy of the nuclear transitions and nuclear fusion. But, instead of a Fermi gas we now have a boson gas consisting of briefly thermalized nucleons. The volume containing the nucleons is the same during SUSY transition.

The results of the previous energy parameters are given in Table 4.4. As one can see the energy output is also consistent with previous calculations and is around 32.38×10^{57} MeV of total energy.

One can observe that the Fermi gas model calculations are giving an extra order of magnitude in energy. This can be explained very simply: in our calculations we used a first order approximation for the binding potential in nuclei. Obviously, a better approximation for the bosonic state potential will be a shallower well with all

the nucleons occupying the lowest level, which will lead to lowering the total energy.

The consistency of the results leads us to the conclusion that collective models can be used as a first order approximation in calculation of the energy of the nuclear reactions in the supersymmetric state.

One can combine the results of the two models to create a liquid drop toy-model for the binding energy of bosonic nucleons. This toy-model is described by the tailored Weizsaecker's formula

$$E_{\mathrm{B}} = \widetilde{a}_V A - a_S A^{2/3} - a_C Z(Z-1)A^{-1/3} - \widetilde{a}_A \frac{(A-2Z)^2}{A}$$

where $\widetilde{a}_V$ and $\widetilde{a}_A$ are modified volume and asymmetry coefficients. According to expansion (4.2) and the fermionic Weizsaecker's formula (4.1) the absolute values of these coefficients are: $\widetilde{a}_V = a_V^{\mathrm{Fermi}} + a_V$ and $\widetilde{a}_A = a_A - a_A^{\mathrm{Fermi}}$. By introducing these corrections and neglecting the δ-term in (4.1) we are removing all fermionic behavior from the liquid drop model. One can also notice that the modified asymmetry coefficient does not vanish for any set of the parameters. That means that a residual asymmetry term is present in the total mass formula. However, the coefficient for the asymmetry term is smaller, leading to weakening the restriction on asymmetry. Hence, the stability island for isotopes is shifted toward the heavier (more neutron-rich) nuclei. The example of such shift for the iron atom is presented in Table 4.5. Since the stable nuclei become heavier in the SUSY state, the total energy output for a transition will increase. However, this model requires closer consideration, which is one of the goals of future work.

Atoms	Decay	2		3		4		5	
		F	B	F	B	F	B	F	B
^{56}Fe	α	-87.07	-20.64	-7.27	-86.91	-7.98	-87.61	-7.74	-87.38
	β	-9.77	-6.44	-70.23	-5.60	-6.78	-6.17	-7.15	-6.32
	β^+	0.02	3.35	-67.82	3.14	-3.97	2.98	-3.97	3.20
	K	1.04	4.37	-66.80	4.16	-2.95	4.00	-2.95	4.22
^{57}Fe	α	-87.41	-20.82	-7.58	-87.09	-8.42	-87.88	-8.19	-87.64
	β	-5.60	-5.60	-1.92	-5.03	-2.16	-5.28	-2.35	-5.46
	β^+	2.53	2.53	-2.08	2.59	-2.55	2.12	-2.30	-2.37
	K	3.55	3.55	-1.06	3.61	-1.53	3.14	-1.28	3.39
^{58}Fe	α	-87.59	-21.00	-7.91	-87.28	-8.79	-88.16	-8.55	-87.92
	β	-8.01	-4.78	-67.65	-4.48	-3.52	-4.41	-3.95	-4.63
	β^+	-1.49	1.74	-70.30	2.06	-7.00	1.29	-6.94	1.57
	K	-0.47	2.76	-69.28	3.08	-5.98	2.31	-5.92	2.59
^{59}Fe	α	-87.97	-21.20	-8.28	-87.49	-9.30	-88.46	-9.06	-88.22
	β	-3.98	-3.98	0.57	-3.94	0.93	-3.58	0.69	-3.82
	β^+	0.98	0.98	-4.47	1.54	-5.53	0.48	-5.22	0.79
	K	2.00	2.00	-3.45	2.56	-4.51	1.50	-4.20	1.81
^{60}Fe	α	-88.19	-21.40	-8.67	-87.70	-9.74	-88.78	-9.49	-88.53
	β	-6.37	-3.22	-65.25	-3.42	-0.48	-2.77	-0.97	-3.04
	β^+	-2.91	0.24	-72.61	1.04	-9.84	-0.30	-9.71	0.04
	K	-1.89	1.26	-71.59	2.06	-8.82	0.72	-8.69	1.06
^{62}Fe	α	-88.83	-21.81	-9.51	-88.16	-10.81	-89.45	-10.54	-89.19
	β	-4.83	-1.75	-63.00	-2.43	2.37	-1.23	1.83	-1.56
	β^+	-4.24	-1.17	-74.78	0.09	-12.49	-1.78	-12.30	-1.38
	K	-3.22	-.015	-73.76	1.11	-11.47	-0.76	-11.28	-0.36
^{63}Fe	α	-89.24	-22.03	-9.96	-88.39	-11.42	-89.80	-11.15	-89.53
	β	-1.06	-1.06	5.08	-1.96	6.55	-0.50	6.19	-0.85
	β^+	-1.84	-1.48	-8.81	-0.36	-10.93	-2.48	-10.51	-2.06
	K	-0.82	-.082	-7.79	0.66	-9.91	-1.46	-9.49	-1.04
^{64}Fe	α	-89.51	-22.24	-10.42	-88.63	-11.95	-90.17	-11.67	-89.89
	β	-3.39	-0.38	-60.88	-1.51	5.05	0.22	4.46	-0.17
	β^+	-5.49	-2.49	-76.81	-0.80	-14.97	-3.17	-14.73	-2.72
	K	-4.47	-1.47	-75.79	0.22	-13.95	-2.15	-13.71	-1.70
^{65}Fe	α	-89.94	-22.46	-10.89	-88.88	-12.59	-90.53	-12.30	-90.25
	β	0.27	0.27	7.13	-1.06	9.10	0.91	8.69	0.50
	β^+	-3.12	-3.12	-10.78	-1.23	-13.39	-3.83	-12.92	-3.36
	K	-2.10	-2.10	-9.76	-0.21	-12.37	-2.81	-11.90	-2.34
^{66}Fe	α	-90.22	-22.68	-11.37	-89.13	-13.15	-90.91	-12.86	-90.61
	β	-2.03	0.91	-58.90	-0.63	7.56	1.58	6.93	1.14
	β^+	-6.67	-3.73	-78.72	-1.64	-17.31	-4.48	-17.02	-3.99
	K	-5.65	-2.71	-77.70	-0.62	-16.29	-3.46	-16.00	-2.97
^{67}Fe	α	-90.65	-22.90	-11.87	-89.38	-13.81	-91.29	-13.51	-90.98
	β	1.53	1.53	9.05	-0.22	11.50	2.23	11.04	1.77
	β^+	-4.32	-4.32	-12.63	-2.04	-15.70	-5.10	-15.18	-4.59
	K	-3.30	-3.30	-11.61	-1.02	-14.68	-4.08	-14.16	-3.57
^{68}Fe	α	-90.95	-23.13	-12.37	-89.64	-14.40	-91.67	-14.09	-91.36
	β	-0.75	2.13	-57.03	0.19	9.93	2.86	9.25	2.38
	β^+	-7.77	-4.90	-80.52	-2.43	-19.51	-5.71	-19.17	-5.17
	K	-6.75	-3.88	-79.50	-1.41	-18.49	-4.69	-18.15	-4.15

Table 4.5: Stability of different isotopes of iron nucleus. Parameters' sets are the same in the chapter. Positive number for energy release (in MeV) implies decay, whereas negative number corresponds to stability against the decay mode. F=fermionic state of nucleons, ordinary matter; B=bosonic state of nucleons, supersymmetric matter

Chapter 5

Discussion and Conclusions

In our work we presented a possible model for the gamma-ray burst origin inside astronomical objects. In this model energy released during SUSY transitions is of the order of magnitude of observable GRBs. This model does not claim to be the only possible explanation for GRB formation. It also can be a good candidate for existing models that lack an internal engine.

In chapter 3 we showed that after the SUSY transition jets are formed due to electron pair conversion. The *s*electron momentum distribution will carry over into the photon momentum distribution since bosons will necessarily fall into the ground state via photon emission. This numerical evaluation of the gamma-ray emission is a primary quantitative result of this part of the work. The secondary result is that the initial spikes in gamma ray bursts would be expected to be of higher photon energy than the later components,which is consistent with observations [38].

Calculations presented in this chapter are primarily relevant to white dwarf evolution. Similar consideration can be given to nucleon pair conversion inside the neutron

stars[1]. These calculations no doubt would be more sophisticated considering the rich spectrum of possible quark-quark, quark-*s*quark and *s*quark-*s*quark interaction. Such calculations are among the future goals in extending the present work.

Some other goals of future investigations are calculations of the gamma-ray spectrum from radiative SUSY conversion and bremsstrahlung from the final state *s*electron gas as well as consideration of polarization effects during the transition.

In chapter four we considered different collective models of nuclei. For all of them and for the different set of model parameters, the total energies of nuclei were calculated and the energy release of the SUSY transition was estimated.

One can argue that all of these models use empirical parameters, that may not be valid for the supersymmetric nuclei. We do agree with this statement, but will argue that for the brief period of time after the transition all of the parameters describing the behavior of supersymmetric partners of ordinary particles remain the same. Hence as a first order approximation the considered models are valid. The energy output of nuclear reactions are of the order of magnitude of the energies of GRBs. This is another positive argument in favor of the suggested model of GRB origin.

One may notice that for the Fermi gas model the total energy output for the nuclear reactions is much higher, than for other models. This could be explained naturally. After the transition all nucleons, being bosons, tend to take the lowest energy level. Hence, overpopulating ground state. In this condition it is reasonable to assume that the size of the nucleus may increase and that will lead to a shallower potential well. Also one may consider a completely different approach - in such a

[1]However the much smaller volume of neutron stars makes the transitions much less likely.

dense environment nucleons may lose spatial uniqueness and become some form of Bose-Einstein condensate. Unfortunately, the theoretical models of such behavior being developed cannot be tested - we live in world of broken supersymmetry. But one can try to develop toy models for this process. This is also one of the possible directions of current research.

References

[1] Johnathan I.Katz, "The Biggest Bangs", Oxford University Press(2002).

[2] B. E. Schaefer *et al*,"Gamma-ray burster counterparts - Infrared", APJ **313**, 226 (1987)

[3] D. Marsden, N. E. White, "Observations of SGRs and AXPs with ASCA", Bulletin of the American Astronomical Society, **32**, 1432 (2000)

[4] http://www.batse.msfc.nasa.gov/batse/

[5] http://gcn.gsfc.nasa.gov/sax_grbs.html

[6] F. Frontera et al., ApJ, 493 (1998) L67

[7] X. Y. Wang, Z. G. Dai and T. Lu, "Intrinsic Parameters of GRB990123 from Its Prompt Optical Flash and Afterglow," Mon. Not. Roy. Astron. Soc. **319**, 1159 (2000) [arXiv:astro-ph/9906062].

[8] N. Masetti, "Near-infrared detection and optical follow-up of the GRB990705 afterglow," arXiv:astro-ph/9912423.

[9] L. Piro *et al.*, Science **290**, 955 (2000) [arXiv:astro-ph/0011337].

[10] K. N. Borozdin and S. P. Trudolyubov, Astrophys. J. **583**, L57 (2003) [arXiv:astro-ph/0205208].

[11] Stephen T. Holland *et al*, "The Optical Afterglow of the Gamma-Ray Burst GRB 011211", The Astronomical Journal **124** 639 (2002)

[12] K. Hurley, "PN triangulation of GRB021223 (two large error boxes)", GRB Coordinates Network, **1778**, 1 (2002)

[13] E. Nakar,T. Piran, J. Granot, "Variability in GRB afterglows and GRB 021004", New Astronomy, **8**, 5 (2003)

[14] Y. M. Lipkin *et al*, "The detailed optical light curve of GRB 030329",Astrophys.J. 606 (2004), [arXiv:astro-ph/0312594v2]

[15] R. Ruffini, "GRB 050315: A step toward the uniqueness of the overall GRB structure", NUOVO CIMENTO- SOCIETA ITALIANA DI FISICA SEZIONE B, **121**, 10/11 (2007)

[16] J. Cummings,*et al* "GRB050502B Swift-BAT refined analysis", GRB Coordinates Network, Circular Service, 3339, 1 (2005)

[17] J. L. Racusin, "GRB 080319B: fit to burst", Nature, 9 (2008)

[18] P. Meszaros,"Gamma-Ray Bursts: Accumulating Afterglow Implications, Progenitor Clues, and Prospects", Science, **291**, 5501, (2001)

[19] G. S. Bisnovatyi-Kogan, "Origin of GRB Afterglows in the Model of Galactic Neutron Stars", [arXiv:astro-ph/9903090]

[20] L. Caito, "GRB060614: a 'fake' short GRB from a merging binary system", Astronomy and Astrophysics, **498**, Issue 2, (2009)

[21] D. H. Hartmann, M. S. Briggs, G. N. Pendleton, J. Hakkila, APSS, 231, 361 (1995)

[22] Xiang-Yu Wang and Peter Mszros, "GRB Precursors in the Fallback Collapsar Scenario", The Astrophysical Journal, 670, (2007)

[23] E. Berger *et al*, "A Merger Origin for Short Gamma-Ray Bursts Inferred from the Afterglow and Host Galaxy of GRB 050724", Nature 438 (2005)[astro-ph/0508115]

[24] R. Ouyed,"Quark Stars and Color Superconductivity: A GRB connection?", [arXiv:astro-ph/0201408v1]

[25] L. Clavelli and G. Karatheodoris, hep-ph/0403227

[26] Bradley W. Carroll and Dale A. Ostlie, "An Introduction to Modern Astrophysics", 2 Ed., Pearson (2008)

[27] S. P. Martin, "A Supersymmetry Primer," arXiv:hep-ph/9709356.

[28] L. Clavelli and I. Perevalova, "Electron to selectron pair conversion in a SUSY bubble," Phys. Rev. D **71**, 055001 (2005) [arXiv:hep-ph/0409194].

[29] W.-Y. Keung and L. Littenberg, Phys. Rev. *D26*, 1067 (1983)

[30] H.E. Haber and G.L. Kane, Phys. Rep. **117**, 75 (1985)

[31] F. Cuypers, G. van Oldenborgh, and R. Ruckl, Nucl. Phys. **B409**, 128, 1993

[32] J. Feng and M. Peskin, Phys. Rev. **D64**, 115002-1

[33] See the summary of monte carlo techniques in Review of Particle Properties, Particle Data Group, Phys. Rev. **66D**, 1 (2002)

[34] K.S. Krane, "Introductory Nuclear Physics", Wiley and Sons (1988)

[35] A. H. Wapstra,"Atomic Masses of Nuclides", Springer, (1958)

[36] James William Rohlf,"Modern Physics from a to Z0", Wiley, (1994)

[37] R.Freedman, H.Young, "University Physics with Modern Physics', 11th international edition, Sears and Zemansky (2004)

[38] E. Pian et al, astro-ph/9910235